Polymer Chemistry

ROYAL SOCIETY OF CHEMISTRY

PAPER

View Article Online
View Journal | View Issue

Cite this: *Polym. Chem.*, 2025, **16**, 4795

Adhesive-tuning with aromatic dithiols in thiol-quinone Michael polyadditions to tailor thiol-catechol connected (TCC) polymers

Ching-Yi Choi, [a] Lukas D. Bangert, [a] Leon Hertweck,[b] André Dallmann, [a] Philipp Woite,[c] Michael Roemelt [c] and Hans G. Börner *[a]

Received 15th July 2025,
Accepted 1st October 2025

DOI: 10.1039/d5py00709g

rsc.li/polymers

Aromatic phenolic dithiol monomers facilitate efficient thiol-quinone polyaddition, thereby expanding the property space of adhesives featuring thiol-catechol connectivities (TCCs). Compared to aliphatic thiols, a cleaner and faster polymerisation is achieved with bisquinone A. Dithiol isomers influence polymerisation kinetics, product glass transition temperatures, and adhesive lap shear strength. Underwater adhesion tests confirm robust bonding, demonstrating the potential for bioinspired performance adhesives.

Introduction

Despite decades of intensive and highly fruitful research in the field of bioinspired adhesives,[1–7] noteworthy advancements continue to be made.[8–16] Among bioadhesive strategies,[17–19] the catechol functionality, present as L-3,4-dihydroxyphenylalanine (Dopa) in sclerotized cuticle proteins and mussel byssal threads,[20,21] has become a central motif in bioinspired adhesives. Dopa provides exceptional interaction properties, thereby enhancing cohesion and enabling wet adhesion to virtually all hard substrates.[22] Since the pioneering work in the 1980s,[23,24] a rich family of catechol-bearing biomimetic polymers has emerged,[25] including minimal motif adhesive peptides, peptide-polymer conjugates, recombinant or artificial adhesive proteins, statistical copolymers and catechol-modified commodity polymers.[26–31] These polymers exhibit remarkable properties including antifouling, redox-switchable, self-healing, and triggerable debonding properties, realizing exciting applications such as universal and substrate-specific coatings, robust (sea)water adhesives, renewable coral glues, biomedical adhesives, and tuneable cell growth scaffolds for tissue engineering.[11,12,32–37]

Recently, a study demonstrated the synthesis of bioinspired adhesives *via* Michael-type polyaddition of thiols and *ortho*-quinones.[38] This route produces thiol-catechol connectivities (TCCs)[39] that mimic the potent and robust adhesive properties of Dopa catechols.[38] The approach is generic and potentially scalable, with quinones being obtained from either (bio) phenols enzymatically,[35] chemically *via* 2-iodoxybenzoic acid (IBX) oxidation,[40] or electrochemically on graphitic electrodes directly from catechols.[41] The thiol-quinone polyaddition has successfully employed peptide-based Tyr-X-Cys (AB-type) unimers.[38] Moreover, a versatile family of bisquinones (AA-type), which can be derived from dityrosine,[12] diDopa or bisphenol commodity monomers,[39] can be effectively copolymerised in solution with dithiols (BB-type).[12,39,42] In addition, multithiols, that constitute a diverse class of building blocks established in the context of thiol–ene/yne and thiol-halogen click chemistries,[43–45] can be applied to thiol-quinone polyaddition as well.[12,41] More recently, lignin activation produced a green multiquinone, which crosslinked with polymeric tri- or tetra-thiol star polymers in a solvent-free two-component (2 K) system to form a strong adhesive resin.[11]

Börner and coworkers reported a library of 40 adhesive TCC polymers by reacting five bisquinones with eight dithiols.[42] So far, TCC polymer synthesis relied on aliphatic thiols, but aromatic thiols (thiophenols) could offer higher reactivity and lead to polymers with reduced segmental flexibility compared to aliphatic or benzylic analogues. Similar advantages are known from aromatic polyamides (aramids), which combine thermal stability, mechanical strength, and high glass transition temperatures (T_gs).[46] Furthermore, monomer substitution patterns modulate polyaramid properties, as shown by the contrast between Nomex® and Kevlar®.[47] Introducing aromatic dithiols into TCC backbones may thus enhance polymerisation rates and T_g, and strengthen both cohesion and adhesion.

Here, we use BB-type dithiophenol monomers such as benzenedithiol (BDT) in thiol-quinone Michael-type polyadditions

[a]*Laboratory for Organic Synthesis of Functional Systems, Department of Chemistry, Humboldt Universität zu Berlin, Brook-Taylor-Str. 2, 12489 Berlin, Germany. E-mail: h.boerner@hu-berlin.de*
[b]*Micro & Nano Analytical Science, Department of Chemistry, School of Analytical Sciences Adlershof (SALSA), Humboldt Universität zu Berlin, Brook-Taylor-Str. 2, 12489 Berlin, Germany*
[c]*Department of Chemistry, Humboldt-Universität zu Berlin, Brook-Taylor-Str. 2, 12489 Berlin, Germany*

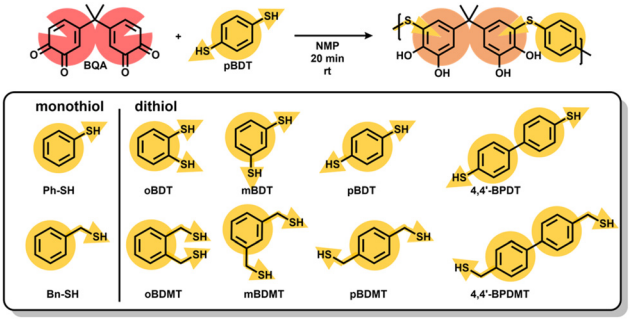

Fig. 1 Schematic illustration of a generic TCC polymerisation (top) exemplified by p(BQA-*p*BDT). Using a combinatorial monomer library (bottom) yields a set of TCC polymers. Bisphenol A is oxidised by iodoxybenzoic acid to bisquinone A as AA-type monomer that reacts in a Michael-type polyaddition with aromatic mono- or dithiols (BB-monomer).

with the AA-type bisquinone A to synthesise aromatic TCC polymers (Fig. 1). The reactivity and selectivity of thiophenol addition were analysed and the influence of *ortho*-, *meta*-, and *para*-substitution in BDT isomers on TCC polymer properties was evaluated and compared to the corresponding benzenedimethanethiol (BDMT) isomers. Moreover, the biphenyl dithiols 4,4′[biphenyl]-dithiol (4,4′BPDT) and the benzylic analogue 4,4′[biphenyl]dimethanethiol (4,4′BPDMT) were incorporated to evaluate the impact of biphenyl unit on adhesive performance.

Results and discussion

The commodity monomer bisphenol A (BPA) can be straightforwardly oxidised by 2-iodoxybenzoic acid (IBX) in MeOH at rt to give bisquinone A (BQA).[39] This product precipitated as a reddish solid directly from the reaction mixture and required no further chromatographic purification. To initially prove the capability of thiophenols (Ph-SH) to react with BQA, a model study with thiophenol as monothiol was conducted in *N*-methyl-2-pyrrolidone (NMP) (Fig. 2a). BQA rapidly reacted with one equivalent of thiol per quinone group at rt, fully consuming the quinones within less than 30 s, as monitored by UV/vis spectroscopy at 381 nm (Fig. 2b). In comparison, the analogous reaction with benzyl thiol (Bn-SH) proceeded significantly slower, requiring approximately 15 min to reach full quinone conversion. The higher reactivity and nucleophilicity of aromatic thiols was expected,[48] and correlates well with the reduced acidity of benzyl thiols ($pK_{a,Ph\text{-}SH} \approx 6.5$, $pK_{a,Bn\text{-}SH} \approx 9.4$).[49]

Ultra-high-performance liquid chromatography mass spectrometry (UHPLC-ESI-MS) analysis of both stoichiometric reactions showed distinct product mixtures of three main compounds (Fig. 2c and d). The disubstituted adduct was found to be the main product for both thiols, whereas the monosubstituted adducts were consistently low in occurrence. Remarkably, thiophenol reacts cleanly with BQA, leading to

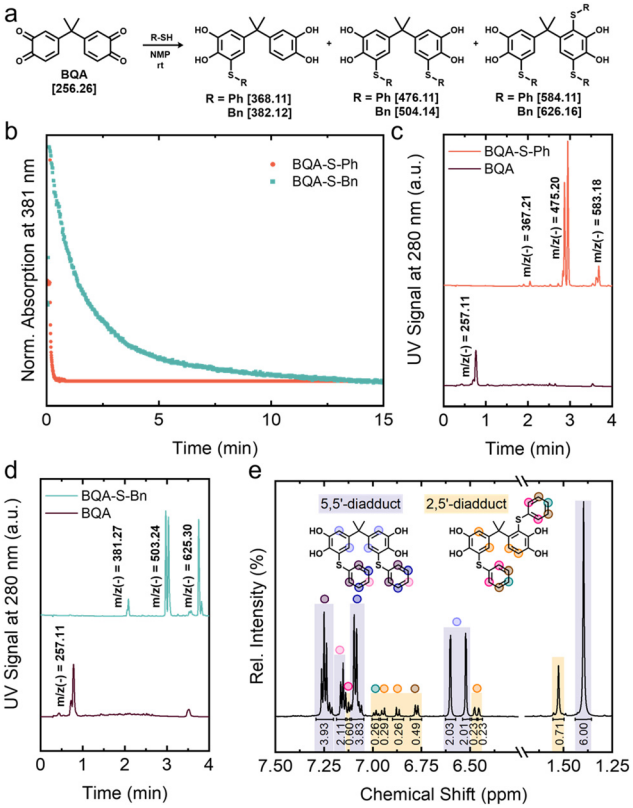

Fig. 2 Michael-type model reactions of BQA with either Ph-SH or Bn-SH. The corresponding exact masses (Da) are shown in brackets (a). UV/vis spectroscopy following the consumption of BQA by monothiols (b). UHPLC UV traces of the reaction mixture of BQA with Ph-SH (c) or with Bn-SH (d) after 12 h reaction (solvent A: water, 0.1% formic acid, solvent B: acetonitrile, 0.1% formic acid, gradient 30–90% B; with BQA reference). ^{1}H NMR spectroscopy of BQA/2Ph-SH reaction assigned to 5,5′-diadducts (violet) and 2,5′-diadducts (yellow) (e).

the desired disubstituted adduct as the majority compound, whereas benzyl mercaptan forms a mixture of di- and trisubstituted products. A rough quantitative estimation could be obtained by normalising the integral intensities of the chromatogram UV traces based on the number of aromatic entities. This analysis suggests a high selectivity and negligible side reactions for thiophenol addition to BQA. While BQA/2Ph-SH gave a roughly estimated ratio of mono/di/trisubstituted products of 1/97/2, the BQA/2Bn-SH exhibited a less favourable ratio of 1/69/30.

For both Ph-SH and Bn-SH reactions, UHPLC-ESI-MS and ^{1}H NMR analyses found predominantly two out of the six possible regioisomeric di-TCC adducts. The signals of BQA-(S-Ph)$_2$ could be assigned to the 5,5′- and 2,5′-di-TCC adducts, with NMR indicating a 9/1 ratio favouring the 5,5′-isomer (Fig. 2e). This regioselectivity mirrors that observed in cysteinyldopa formation, where the 5-S isomer dominates the product mixture.[50] The more nucleophilic thiophenols facilitate the rapid Michael-type addition compared to the benzylic thiols, thereby limiting oxidative transfer from quinone to TCC-catechol and effectively suppressing undesired over-substitution.[51,52]

The chemical identities of both disubstituted TCC products were confirmed by mass spectrometry using UHPLC-ESI-MS in negative ionization mode. The detected molecular ions matched well the theoretical masses of BQA-$(S\text{-}Ph)_2$ (476.11 Da; found m/z 475.20) and BQA-$(S\text{-}Bn)_2$ (504.14 Da; found m/z 503.24) in the respective reaction mixtures. Structural confirmation of the TCC motif in the BQA/2Bn-SH reaction product was provided by 2D NMR spectroscopy. ^{1}H–^{13}C HSQC and HMBC experiments revealed a distinct ^{3}J-coupling between the benzylic CH_2 protons and the aromatic carbon of the BQA unit ($C_{Ar,BQA}$) across the thioether linkage.[39] In contrast, the TCC structure in the BQA$(S\text{-}Ph)_2$ product could only be inferred indirectly, as ^{4}J-couplings were expected between the thiophenol moiety and the BQA core.[53] Nevertheless, the ^{1}H NMR spectrum showed four distinct aromatic signals, allowing separation of thiophenol- and BQA-derived protons. Assignments were supported by ^{1}H–^{13}C HSQC and HMBC, where correlations between BQA aromatic protons and its methyl carbons confirmed their origin (SI Fig. S24). Notably, the signals of the thiophenol moiety display only ^{1}J-, ^{2}J- and ^{3}J-couplings within that moiety, suggesting structural isolation. Complementary diffusion-ordered spectroscopy (DOSY) showed identical diffusion coefficients for protons from both distinct aromatic moieties, thereby verifying that the CH_3 groups of the BQA unit and aromatic C–H protons of the thiophenol unit belong to the same molecular entity (SI Fig. S26).

The model reaction successfully confirmed the Michael-type addition of thiophenols to BQA, proving both higher reactivity and selectivity compared to benzyl mercaptans. These effects are expected to benefit the polyaddition reaction required to produce high-molecular-weight TCC polymers.

As expected, the reactivity of *ortho*-, *meta*-, and *para*-dithiol phenols varied significantly. Upon addition of *m*BDT or *p*BDT, the polymerisation mixture changed colour within seconds from dark red to light yellow, indicating rapid quinone consumption. In contrast, the *ortho*-isomer *o*BDT showed no full discolouration, though immediate discolouration upon ethanethiol addition confirmed the presence of reactive BQA and suggested hindered, incomplete polymer growth in case of *o*BDT. Steric effects in *o*BDT could be expected and likely favour fold-back conformations limiting growth to low-molecular-weight species, as suggested by size exclusion chromatography (SEC) analysis (SI Fig. S27 and S28).[54] This is in accordance with the literature, describing a difficult growth step for *ortho*-substituted benzene-dinucleophiles, compared to their *para*- and *meta*-substituted counterparts.[55–57] Interestingly, DFT calculations could not reveal significant kinetic differences between the *para*- and *ortho*-isomers in the initial two addition steps (SI Scheme S1, Table S1 and S2). However, the limited molecular weight of p(BQA-*o*BDT), reaching only M_w of 2500 g mol^{-1}, indicated that chain growth slows down at later stages. This reduced reactivity might be rationalised by steric hindrance, where backfolding of *o*BDT-containing chains progressively limits accessibility of the reactive chain ends.

To investigate the influence of stoichiometry of the functional groups on the molecular weight of TCC polymer products, an AA + BB (bisquinone + dithiol) polyaddition reaction in NMP was carried out by slightly varying quinone equivalents from 0.90 to 1.05 with respect to thiols in the *p*BDT (Fig. 3a). The polymerisation proceeds in a nearly ideal manner, as evidenced by the highest molecular weights observed at a quinone-to-thiol (Q/T) ratio of 0.95/1.05–1.00/1.00. This highlights the robustness of the polyaddition process, with the optimal functionality ratio remaining constant across various dithiols, including thiophenols, and benzyl analogues (Fig. 3b and SI Fig. S29). According to Carothers' equation for AA/BB polyadditions, deviations from ideal stoichiometry lowered the molecular weight of the TCC polymers products.[58] Interestingly, the polymerisation tolerated excess of thiol more effectively than quinone excess, potentially suggesting that under thiol-rich conditions, disulfide formation might buffer thiol overabundance *via* an alternative growth pathway.

Consistent with the UV/vis kinetics, the polymer growth in the BQA/*p*BDT solution polyaddition at a Q/T ratio of 1.00/1.00 levelled off within about 15 seconds, as indicated by SEC. Over a period of 4 hours, no significant increase in molecular weight was found (Fig. 3c). The SEC trace exhibited only a marginal and rather symmetric shift, with the peak molecular weight (M_p) increasing by approximately 400 g mol^{-1} from 15 seconds to 4 hours. In agreement with the literature and the model reaction, the solution polyaddition of BQA with *p*BDMT proceeded much slower than that of *p*BDT. The primary growth occurred within the first 15 minutes, with only a minor increase over the subsequent 4 hours (Fig. 3c). Under comparable conditions, *p*BDT underwent the polyaddition reaction significantly faster, yielded polymers with notably higher M_p

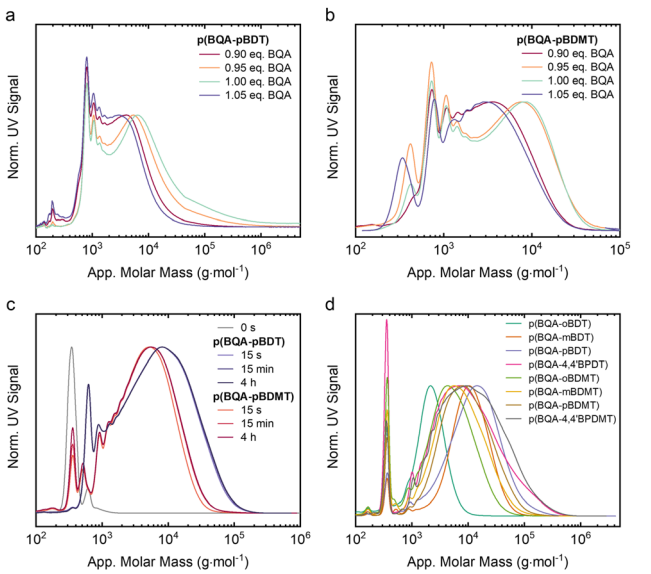

Fig. 3 SEC analyses of p(BQA-*p*BDT) and p(BQA-*p*BDMT) synthesised at varying AA/BB monomer feed ratios (0.90 to 1.05 equivalents BQA) (a and b). Kinetic studies of p(BQA-*p*BDT) and p(BQA-*p*BDMT), monitoring polymer growth over time (c). SEC analysis of isolated and purified TCC polymers (d) (c and d conditions: Q/T = 1.00/1.00, *c*[BQA] = 0.15 mol L^{-1}, NMP, rt).

and with high molecular weight flanks reaching up to 5×10^5 g mol^{-1}. These results demonstrate that dithiophenols can be added to the pool of feasible BB-type monomers, thereby expanding the scope of the thiol-quinone Michael-type polyaddition.

To reveal structure–property relationships, a material library of eight different TCC polymers was synthesised in a straightforward manner. Solution polymerisation was conducted at a BQA concentration of 0.15 mol L^{-1} in NMP, yielding the set of TCC polymers. All products were isolated by precipitation from methanol, where undesired low molecular weight materials could be fractionated (Table 1 and Fig. 3d). In addition to employing the previously mentioned dithiophenols and their benzylic analogues, the study also included biphenyl-based dithiols such as 4,4′[biphenyl]-dithiol (4,4′BPDT) and 4,4′-[biphenyl] dimethanethiol (4,4′BPDMT), to expand the structural space of the TCC polymer library. Isolated yields were typically 60–80%, though for low molecular weight products like p(BQA-*o*BDT) only 30% could be recovered as precipitate. The chemical structures of the purified TCC polymers were comprehensively characterised by SEC, Matrix-assisted laser desorption/ionisation time-of-flight mass spectrometry (MALDI-TOF MS), NMR and FTIR (*cf.* SI). Structural analysis was exemplified using p(BQA-*p*BDT), as illustrated in Fig. 4.

^{1}H NMR spectroscopy confirmed the stoichiometric ratio of the inbuilt AA/BB monomers within the error of the method (Fig. 4a and SI). Moreover, despite the non-trivial desorption of p(BQA-*p*BDT), MALDI-TOF MS analysis displayed a homologous series of mass signals with alternating peak distances corresponding to the AA-BB mass patterns expected of a BQA (258.09 Da) and *p*BDT (139.98 Da) backbone (Fig. 4b, and SI). FTIR spectroscopy suggested full consumption of quinones, as the characteristic vibration band of 1660 cm^{-1}, typical to conjugated carbonyls in the quinone, vanished (Fig. 4c, and SI). The SEC analysis of p(BQA-*p*BDT) revealed high apparent molar weights of $M_{w,app}$ = 22 000 g mol^{-1} with a dispersity of $Đ$ = 2.8 and a pronounced high molecular weight flank reaching M_{max} up to 5×10^5 g mol^{-1} (Table 1).[58] No evidence for an alternative disulfide-mediated growth was found, as tributylphosphine addition, which cleaves potential disulfide linkages, did not alter the SEC traces significantly (Fig. 4d).

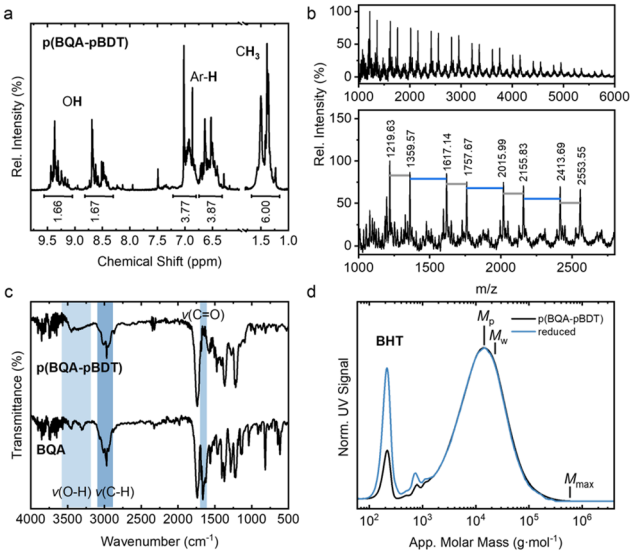

Fig. 4 Characterisation of p(BQA-*p*BDT) including ^{1}H NMR spectroscopy in DMSO (a), MALDI-TOF MS analysis of adducts: 1219.63 *m/z*, 1359.57 *m/z*, 1617.14 *m/z*, 1757.67 *m/z*, 2015.99 *m/z*, 2155.83 *m/z*, 2413.69, 2553.55 *m/z*; calc.: 1219.13 *m/z*, 1359.17 *m/z*, 1617.26 *m/z*, 1757.23 *m/z*, 2015.33 *m/z*, 2155.30 *m/z*, 2413.39 *m/z*, 2553.37 *m/z* (b), FTIR analysis comparing start material BQA and TCC product (c) and SEC analysis of p(BQA-*p*BDT) after using reducing agent for potential disulfide cleavage. M_{max} is the maximum detectable molecular weight at 1% SEC trace intensity (d).

In the entire TCC library, the polymer formation across the set of monomers proceeded *via* a thiol-quinone Michael-type addition mechanism, yielding alternating AA-BB-type polyaddition products. Nonetheless, SEC analysis revealed distinct effects of the three different classes of dithiol monomers, as well as their respective isomers, on the molecular weight of the resulting TCC polymers (Table 1). Apparently, *para*-substituted monomers consistently yield the highest $M_{w,app}$ and M_{max}, which can be attributed to a linear geometry resulting in low steric hindrance and promoting efficient chain propagation. In contrast, *ortho*-substituted analogues reached significantly lower molecular weights due to steric congestion that renders polymer growth less favourable. The *meta*-substituted monomers show an intermediate behaviour and balance steric effects with backbone distortion. BDT-based polymers generally reach higher molecular weights than their BDMT counterparts, suggesting that both the increased planarity of the structural element and the higher reactivity of the thiophenols promote effective polymerisation. Solely the *ortho*-isomer of BDMT shows superior performance when compared to *o*BDT as the higher flexibility compensates for steric constraints. Thus, the use of *o*BDT was discontinued, as only oligomers were obtained, which appeared unsuited for adhesive applications. The highest molecular weights were observed in the 4,4′-disubstituted biphenylic monomers, p(BQA-4,4′BPDT) and p(BQA-4,4′BPDMT). This might be explained by the higher

Table 1 Overview on the SEC, DSC and TGA analyses of the purified TCC polymers

	M (kg mol^{-1})				T (°C)	
TCC polymers	M_p [a]	$M_{w,app}$ [b]	M_{max} [b]	$Đ$ [b]	T_g [b]	$T_{5\%}$ [b]
p(BQA-*o*BDT)	n.d.	2.5	n.d.	n.d.	n.d.	n.d.
p(BQA-*m*BDT)	n.d.	14.0	90	1.7	142	300
p(BQA-*p*BDT)	8.2	22.0	500	2.8	153	269
p(BQA-4,4′BPDT)	11.0	23.0	500	3.2	167	327
p(BQA-*o*BDMT)	n.d.	6.9	70	1.3	111	185
p(BQA-*m*BDMT)	n.d.	10.0	100	2.3	107	136
p(BQA-*p*BDMT)	5.6	15.0	200	3.2	121	190
p(BQA-4,4′BPDMT)	5.0	23.0	600	3.2	145	192

M_{max} is maximum detectable molecular weight at 1% SEC trace intensity. [a] Determined from polymerisation mixture after 4 h. [b] Purified by precipitation from methanol; n.d. – not determined.

molecular weights of the 4,4′BPDT and 4,4′BPDMT monomer units compared to their BDT and BDMT analogues but also could reflect a favourable effect of extended conjugation and backbone planarity on polymer growth.

The thermal stability of the TCC polymer set was evaluated by thermogravimetric analysis (TGA, *cf.* Table 1). The results clearly demonstrated that polymers containing phenolic dithiol backbones possess markedly higher thermal resistance, having a 5 wt% mass loss temperatures ($T_{5\%}$) in the range of 270–300 °C. In contrast, TCC polymers with benzyl dithiol units show substantially lower $T_{5\%}$ values between 140 and 190 °C. Interestingly, despite these differences in initial degradation temperatures, the maximum degradation rates of all TCC polymers fall within a similar range of 300–340 °C, suggesting analogous final decomposition pathways. This aligns well with previous studies on aliphatic TCC polymers, indicating that TCC decomposition occurs above 300 °C.[42]

The TCC polymers with phenyl-dithiol backbones also exhibited notably high glass transition temperatures (T_g) of 142–153 °C, as determined by differential scanning calorimetry (DSC, *cf.* Table 1). In contrast, benzylic analogues showed lower T_g values, ranging from 107 °C to 121 °C. However, in both sets, the *para*-isomers consistently reached the highest T_g and the introduction of conformational kinks into the polymer backbone lowered T_g. As anticipated, TCC polymers derived from biphenylic thiophenols reached the highest T_g in the entire set with 167 °C, similar to the *p*BDT product, due to increased structural rigidity. Conversely, the benzylic biphenyl analogue (4,4′BPDMT) with increased segmental flexibility relative to 4,4′BPDT gave a T_g of 145 °C.

These thermal property variations align with known structure–property relationships, as seen *e.g.* in *para*-linked aromatic polyamides (polyaramids), which exhibit higher thermal and mechanical performance than their *meta*-substituted analogues.[46] The *para*-based polyaramids typically achieve high T_g due to symmetric segments enabling strong secondary chain interactions.[59] Similarly, the TCC polymer library shows T_g increases driven by segmental rigidity, molecular symmetry, intermolecular interactions, and chain-end concentrations.[60,61] Taking the low molecular weight model reactions into account, the thiophenol-quinone coupling generally proceeded in a regioselective manner, with only ~10% of 2,5′-isomer defects. DSC analysis consistently showed a single glass transition for each polymer, with no evidence of microphase separation, suggesting that 2,5′-linkages are statistically distributed within the polymer chains rather than forming segregated regions. Given the intrinsically kinked repeat-unit structure of TCC polymers, a comparatively small number of regioisomeric defects might have limited effects on chain packing. By contrast, variations in mono-, di-, and trisubstitution patterns at the bisquinone core are expected to exert a much stronger impact on bulk properties by altering chain topology. Notably, the model reactions showed superior substitution-pattern selectivity for thiophenols (PhSH) compared to benzylthiols (BnSH). Thus, direct consequences on key TCC polymer properties such as melt viscosity and processability are more likely to arise from substitution pattern effects than from regioisomeric differences.

The glass transition temperature can significantly affect the adhesion performance of glues by influencing, for instance, the formation of the adhesive interface, the cohesive bulk strength, and the brittleness of failure modes. Accordingly, the set of TCC polymers was evaluated as "hot-melt"-like adhesives through lap shear tests conducted at room temperature using aluminium substrates (Fig. 5a). The polymer was dissolved in acetone (167 mg mL^{-1}), and 50 µL of the solution was applied to a 7 × 20 mm^2 area. After solvent evaporation at rt, curing was carried out at temperatures 10 °C higher than T_g for 16 minutes.

Apparently, the adhesion strength improved with both increasing $M_{w,app}$ and T_g (Fig. 5b and c). However, a global parameter correlation revealed a wider association between adhesive shear strength and increased T_g, but a weaker dependency on higher molecular weight. For instance, p(BQA-*m*BDT) and p(BQA-4,4′BPDMT) displayed comparable glass transition temperatures (T_g = 142 °C *vs.* 145 °C, respectively) and both achieved high shear strengths (3.3 ± 0.5 MPa *vs.* 2.6 ± 0.5 MPa), despite a substantial difference in their apparent molecular weights ($M_{w,app}$ = 14 000 g mol^{-1} *vs.* 23 000 g mol^{-1}, respectively). Moreover, p(BQA-*p*BDMT) and p(BQA-*m*BDT), which exhibited similar $M_{w,app}$ (~14 000–15 000 g mol^{-1}) but differed significantly in T_g (121 °C *vs.* 142 °C), yielding shear strengths of 1.4 ± 0.3 MPa *vs.* 3.3 ± 0.5 MPa, respectively.

This suggests that chain entanglements are not the primary factor governing adhesive performance. All TCC adhesives left

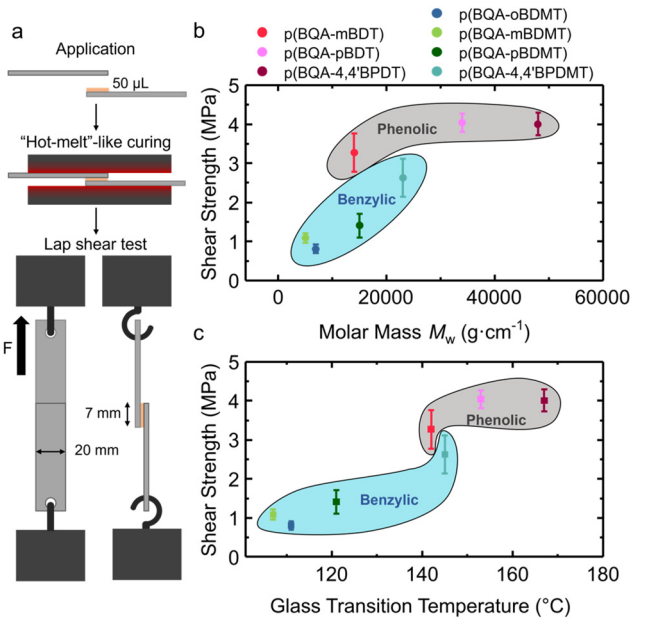

Fig. 5 Performance analysis and testing of seven TCC adhesives by bonding aluminium substrates. Schematic lap shear test setup (a) and global property correlation plots comparing adhesive strength with $M_{w,app}$ (b) and T_g (c). (Data points represent the average. Error bars indicate the standard deviation of the tested samples with n = 6 and the background colour in b & c is only to guide the eye.)

residues on both aluminium substrates after fracture, which appeared in Scanning electron microscope (SEM) images as a finely structured ablation film (SI Fig. S35). Complementary energy-dispersive X-ray spectroscopy (EDX) analysis of the surfaces confirmed the presence of TCC polymers through the detection of sulphur K-band signals, denoted as "positive" in the figure. Together, these observations indicate a mixed failure mode dominated by cohesive domain fracture and suggest strong interfacial adhesion. This supports the assumption that cohesive strength is mainly governed by secondary chain–chain interactions, rather than mechanical entanglements, which would otherwise result in more robust network integrity.

As anticipated, the high chain symmetry in p(BQA-*p*BDT) leads to a high T_g and excellent adhesion performance, reaching a shear strength of 4.0 ± 0.2 MPa. Similarly, increased segmental rigidity introduced by the biphenyl core[62] in p(BQA-4,4′BPDT) yields the highest T_g among the thiophenol derived TCC-polymers and enables a comparable adhesion strength of 4.0 ± 0.3 MPa. This trend is supported by the benzylic thiol derivative with a biphenyl core, which also exhibited a high T_g, and achieved highest shear strengths within the benzylic set at 2.6 ± 0.5 MPa. Overall, phenolic BDT and 4,4′BPDT based TCC polymers show superior T_g and deliver shear strengths up to 4 MPa, which is ∼40% higher than the best performing aliphatic TCC polymer from previous studies (2.4 ± 0.4 MPa).[42] Further comparative bulk mechanical analysis remains challenging, as classical stress–strain tests do not capture the thin-film geometry of adhesive joints, where interfacial effects, physical substrate anchoring, and layer thickness strongly influence the effective properties of the adhesive layer. Nevertheless, the new set of TCC polymers follows general trends observed in previous studies on TCC adhesives, with rigid, hydrophobic materials achieving higher and more durable adhesion strengths than their softer, more hydrophilic counterparts.[12,63]

Given that the class of TCC adhesives are inspired by catechols found in the adhesive systems of marine mussel, evaluating their performance under seawater conditions is of particular interest. Accordingly, the two most promising candidates were selected for underwater performance testing. Protocols based on Wilker *et al.* were adapted to simulated seawater conditions (35 g L^{-1} salinity, 599 mM NaCl).[64] The viscous TCC polymer solutions were applied underwater to aluminium substrates, joined, and cured for 3 days at 50 °C under accelerated curing conditions. Lap shear tests were conducted after air-drying at room temperature. While p(BQA-*p*BDT) showed decent underwater adhesion strengths of 1.6 ± 0.3 MPa, the p(BQA-4,4′BPDT) adhesive exhibited rather impressive 3.4 ± 0.6 MPa, which meets the range of fully formulated commodity epoxy resin underwater adhesives (3.8 ± 0.4 MPa).[11] The p(BQA-*p*BDT) retains only ∼40% of the dry adhesion strength under seawater conditions, whereas p(BQA-4,4′BPDT) retains ∼85%. The shorter *p*BDT linker increases the density of TCC sites, which enhances substrate interactions but simultaneously raises hydrophilicity, promoting water and ion uptake that weakens cohesion. In contrast, the biphenyl-based 4,4′BPDT segment is more hydrophobic, resulting in a greater spatial separation of TCC sites and thus reducing water interactions while preserving cohesion through rigid, glassy biphenyl domains.

A similar trend was observed for the benzylic analogues p(BQA-*p*BDMT) and p(BQA-4,4′BPDMT) cured under seawater conditions (SI Table S3 and Fig. S36). None of the benzylic systems formed robust bonds, as most samples disintegrated upon minimal mechanical stress and consistently exhibited cohesive failures. Only the biphenylic derivative p(BQA-4,4′BPDMT) produced measurable shear strengths of ∼0.9 ± 0.2 MPa. As in the case of the benzylic TCC polymers, the weak bonding performance can be likely attributed to water swelling of the polymer, giving overall weaker network structure due to more flexible benzyl-derived TCC adhesives. These factors explain the uniform occurrence of cohesive failure across benzylic samples and, in direct contrast, rationalise the superior underwater performance of the more rigid biphenyl-based p(BQA-4,4′BPDT).

Direct comparison to previously reported aliphatic TCC polymers shows that the aromatic p(BQA-4,4′BPDT) demonstrates significantly improved wet adhesion strengths.[42] The aromatic backbone probably reduces water interference at the adhesive interface, improving bonding under wet conditions. Interestingly, the biphenyl-based 4,4′BPDT outperforms the BDT unit by a factor of two. This is likely due to the biphenyl unit that reduces hydrophilicity of the bulk and improves cohesive interactions under aqueous conditions *via* entropy driven hydrophobic contacts.[63] Thus, p(BQA-4,4′BPDT) achieves 85% of the shear strength found under dry conditions, which is particularly remarkable, as salt water adhesion is typically significantly weakened compared to a dry-state performance test.[65] Swelling resistance was evaluated by immersing dry-cured samples of p(BQA-*p*BDT) and p(BQA-4,4′BPDT) in water for four days and comparing their shear strengths with those obtained from wet application and underwater curing. The results showed that both polymers retained adhesion within a comparable range, irrespective of the preparation method. For p(BQA-*p*BDT), shear strength decreased only marginally from 1.6 ± 0.3 MPa (direct wet application) to 1.4 ± 0.3 MPa after water immersion. Similarly, p(BQA-4,4′BPDT) maintained 3.0 ± 0.4 MPa after water immersion, close to 3.4 ± 0.6 MPa measured for direct underwater application. Comparative SEM images of the fracture surfaces, combined with EDX analysis, revealed no dramatic influence of swelling on fracture behaviour, demonstrating good stability of both polymers in aqueous environments. The fractures remained predominantly cohesive in nature, and sulphur K-bands were consistently detected, confirming the presence of TCC polymer residues on both substrate sides (SI Fig. S38).

These findings highlight the critical role of T_g in adhesion performance and suggest that, under the given conditions, M_w has a less significant effect in the case of TCC polymers. Obviously, the benzenedithiol and, in particular, the biphenylic analogue, excel at wet adhesion, likely due to an

enhanced hydrophobic nature reducing water interference at the adhesive interface.

Conclusions

Aromatic dithiols have proven to be a most suitable monomer class for thiol-quinone Michael-type polyadditions with bisquinone A (BQA), reacting faster and and generating the desired 5,5′-disubstitution pattern more selectively, when compared to their benzylic analogues. The resulting thiol-catechol connectivities (TCCs) form rapidly in solution, with polymer growth reaching completion within ~15 seconds, in contrast to 15 minutes for benzylic monomers under similar conditions. *ortho*-, *meta*-, and *para*-Phenyldithiol isomers expectedly showed T_g properties known from fully aromatic polyaramids with respect to rigidity and glass transition temperature (T_g). The *para*-isomer of benzenedithiol (BDT) performed the best, producing TCC polymers with $M_{w,app}$ of up to 22 000 g mol^{-1} with high molecular flanks up to $M_{max} = 5 \times 10^5$ g mol^{-1}. The polymer exhibited remarkable thermal stability with a $T_{5\%}$ decomposition temperature of 270 °C, and a T_g of 153 °C. The *meta*-isomer also led to adhesive polymers with slightly reduced T_g due to disturbed backbone symmetry, while the *ortho*-isomer resulted in only lower molecular weight oligomers.

A library of seven TCC polymers, derived from *meta*- and *para*-BDT, *ortho*-, *meta*-, *para*-benzenedimethanethiols (BDMT), and the biphenyl-based dithiols 4,4′[biphenyl]-dithiol (4,4′ BPDT) and 4,4′[biphenyl]dimethanethiol (4,4′BPDMT), was synthesised to enable detailed structure–property analysis. Adhesion studies indicated that both molecular weight and T_g influence adhesion strength, with T_g being the dominant factor. The p(BQA-4,4′BPDT) TCC adhesive reached the highest shear strength on aluminium (4.0 ± 0.3 MPa). In wet adhesion tests in saltwater (599 mM NaCl), 85% of dry adhesive performance could be retained, yielding shear strengths of up to 3.4 MPa. This underlines the suitability of this new class of thiophenol monomers to realise segment rigidity and hydrophobicity, which are key properties for TCC adhesives.

Author contributions

C-YC: investigation, experiments, data analysis, writing, correction; LDB, LH, AD: materials analysis, data curation, methodology development; PW, MR: DFT calculations, data curation, methodology development; HGB: conceptualisation, supervision, funding, resources, validation, writing, reviewing, correcting.

Conflicts of interest

There are no conflicts to declare.

Data availability

The data supporting this article have been included as part of the supplementary information (SI). Supplementary information is available. See DOI: https://doi.org/10.1039/d5py00709g.

Acknowledgements

HGB acknowledges the financial support by the German Federal Ministry of Education and Research (BMBF) within the project "LigNovolac – Fusing material concepts from wood and mussels" grant no 13XP5150 and by the German Reseach Council (DFG) BiPhenOx2TCC BO1762/14-1 (no. 536607484). We thank C. Hansen (HU) for MALDI measurements.

References

1 B. P. Lee, P. B. Messersmith, J. N. Israelachvili and J. H. Waite, *Annu. Rev. Mater. Res.*, 2011, **41**, 99–132.
2 M. J. Sever, J. T. Weisser, J. Monahan, S. Srinivasan and J. J. Wilker, *Angew. Chem., Int. Ed.*, 2004, **43**, 448–450.
3 M. D. Bartlett, A. B. Croll, D. R. King, B. M. Paret, D. J. Irschick and A. J. Crosby, *Adv. Mater.*, 2012, **24**, 1078–1083.
4 H. Lee, S. M. Dellatore, W. M. Miller and P. B. Messersmith, *Science*, 2007, **318**, 426–430.
5 J. Li, A. D. Celiz, J. Yang, Q. Yang, I. Wamala, W. Whyte, B. R. Seo, N. V. Vasilyev, J. J. Vlassak, Z. Suo and D. J. Mooney, *Science*, 2017, **357**, 378–381.
6 C. Greiner, A. Del Campo and E. Arzt, *Langmuir*, 2007, **23**, 3495–3502.
7 L. D. Bangert, N. Kirchner, C.-Y. Choi, M. Biesalski and H. G. Börner, *ACS Appl. Mater. Interfaces*, 2025, **17**, DOI: 10.1021/acsami.5c13781.
8 C. R. Westerman, B. C. McGill and J. J. Wilker, *Nature*, 2023, **621**, 306–311.
9 S. Pal, J. Shin, K. DeFrates, M. Arslan, K. Dale, H. Chen, D. Ramirez and P. B. Messersmith, *Science*, 2024, **385**, 877–883.
10 M. S. A. Bhuiyan, J. Manuel, F. Razaviamri and B. P. Lee, *ACS Appl. Polym. Mater.*, 2023, **5**, 3949–3957.
11 C.-Y. Choi, F. Lossada, K. Walter, T. Fleck-Kunde, S. Behrens, T. Meinelt, J. Falkenhagen, M. Hiller, H. Oschkinat, A. Dallmann, A. Taden and H. G. Börner, *Green Chem.*, 2024, **26**, 2044–2058.
12 T. J. Neubert, K. Walter, C. Schröter, V. Guglielmotti, K. Hinrichs, S. Reinicke, A. Taden, K. Balasubramanian and H. G. Börner, *Angew. Chem., Int. Ed.*, 2024, **63**, e202408441.
13 J. H. Waite and M. J. Harrington, *Can. J. Chem.*, 2022, **100**, 197–211.
14 J. J. Wilker, *Science*, 2021, **374**, 148–150.

15 S. Wei, W. Lu, X. Le, C. Ma, H. Lin, B. Wu, J. Zhang, P. Theato and T. Chen, *Angew. Chem.*, 2019, **131**, 16389–16397.
16 Z. Wang, M. Lin, C. Bonduelle, R. Li, Z. Shi, C. Zhu, S. Lecommandoux, Z. Li and J. Sun, *Biomacromolecules*, 2020, **21**, 3411–3419.
17 P. M. Favi, Y. Sijia, S. C. Lenaghan and M. Zhang, *J. Adhes. Sci. Technol.*, 2014, **28**, 290–319.
18 A. H. Hofman, I. A. van Hees, J. Yang and M. Kamperman, *Adv. Mater.*, 2018, **30**, 1704640.
19 T. B. H. Schroeder, J. Houghtaling, B. D. Wilts and M. Mayer, *Adv. Mater.*, 2018, **30**, 1705322.
20 S. O. Andersen, *Insect Biochem. Mol. Biol.*, 2010, **40**, 166–178.
21 J. H. Waite, *J. Exp. Biol.*, 2017, **220**, 517–530.
22 J. Saiz-Poseu, J. Mancebo-Aracil, F. Nador, F. Busqué and D. Ruiz-Molina, *Angew. Chem., Int. Ed.*, 2019, **58**, 696–714.
23 J. H. Waite and M. L. Tanzer, *Science*, 1981, **212**, 1038–1040.
24 H. Yamamoto and T. Hayakawa, *Polymer*, 1977, **18**, 979–983.
25 J. Sedó, J. Saiz-Poseu, F. Busqué and D. Ruiz-Molina, *Adv. Mater.*, 2013, **25**, 653–701.
26 Y. Li, J. Cheng, P. Delparastan, H. Wang, S. J. Sigg, K. G. DeFrates, Y. Cao and P. B. Messersmith, *Nat. Commun.*, 2020, **11**, 3895.
27 L. Fischer, A. K. Strzelczyk, N. Wedler, C. Kropf, S. Schmidt and L. Hartmann, *Chem. Sci.*, 2020, **11**, 9919–9924.
28 P. Wilke and H. G. Börner, *ACS Macro Lett.*, 2012, **1**, 871–875.
29 S. Arias, S. Amini, J. Horsch, M. Pretzler, A. Rompel, I. Melnyk, D. Sychev, A. Fery and H. G. Börner, *Angew. Chem., Int. Ed.*, 2020, **59**, 18495–18499.
30 M. Yu and T. J. Deming, *Macromolecules*, 1998, **31**, 4739–4745.
31 C. R. Matos-Pérez, J. D. White and J. J. Wilker, *J. Am. Chem. Soc.*, 2012, **134**, 9498–9505.
32 S. Peplau, T. J. Neubert, K. Balasubramanian, J. Polleux and H. G. Börner, *Macromol. Rapid Commun.*, 2023, **44**, 2300300.
33 M. S. A. Bhuiyan, J. D. Roland, B. Liu, M. Reaume, Z. Zhang, J. D. Kelley and B. P. Lee, *J. Am. Chem. Soc.*, 2020, **142**, 4631–4638.
34 B. K. Ahn, D. W. Lee, J. N. Israelachvili and J. H. Waite, *Nat. Mater.*, 2014, **13**, 867–872.
35 P. Wilke, N. Helfricht, A. Mark, G. Papastavrou, D. Faivre and H. G. Börner, *J. Am. Chem. Soc.*, 2014, **136**, 12667–12674.
36 W. Zhang, R. Wang, Z. Sun, X. Zhu, Q. Zhao, T. Zhang, A. Cholewinski, F. Yang, B. Zhao, R. Pinnaratip, P. K. Forooshani and B. P. Lee, *Chem. Soc. Rev.*, 2020, **49**, 433–464.
37 Y. Lee, H. J. Chung, S. Yeo, C.-H. Ahn, H. Lee, P. B. Messersmith and T. G. Park, *Soft Matter*, 2010, **6**, 977–983.
38 J. Horsch, P. Wilke, M. Pretzler, S. Seuss, I. Melnyk, A. Fery, A. Rompel and H. G. Börner, *Angew. Chem., Int. Ed.*, 2018, **57**, 15728–15732.
39 J. M. Krüger and H. G. Börner, *Angew. Chem., Int. Ed.*, 2021, **60**, 6408–6413.
40 R. Bernini, M. Barontini, F. Crisante, M. C. Ginnasi and R. Saladino, *Tetrahedron Lett.*, 2009, **50**, 6519–6521.
41 T. J. Neubert, M. M. Hielscher, K. Walter, C. M. Schroter, M. Stage, R. R. Rosencrantz, F. Panis, A. Rompel, K. Balasubramanian, S. R. Waldvogel and H. G. Börner, *Angew. Chem., Int. Ed.*, 2025, e202419684, DOI: 10.1002/202419684.
42 J. M. Krüger, C.-Y. Choi, F. Lossada, P. Wang, O. Löschke, D. Auhl and H. G. Börner, *Macromolecules*, 2022, **55**, 989–1002.
43 S. Chatani, M. Podgórski, C. Wang and C. N. Bowman, *Macromolecules*, 2014, **47**, 4894–4900.
44 N. Van Herck, D. Maes, K. Unal, M. Guerre, J. M. Winne and F. E. Du Prez, *Angew. Chem., Int. Ed.*, 2020, **59**, 3609–3617.
45 V. P. Beyer, B. Cattoz, A. Strong, D. J. Phillips, A. Schwarz and C. R. Becer, *Polym. Chem.*, 2019, **10**, 4259–4270.
46 J. M. García, F. C. García, F. Serna and J. L. de la Peña, *Prog. Polym. Sci.*, 2010, **35**, 623–686.
47 V. Gabara, in *Ullmann's Encyclopedia of Industrial Chemistry*, 2016, pp. 1–22, DOI: 10.1002/14356007.a13_001.pub2.
48 G. Bosica, R. Abdilla and A. Petrellini, *Organics*, 2023, **4**, 86–96.
49 T. J. Wallace, A. Schriesheim and W. Bartok, *J. Org. Chem.*, 1963, **28**, 1311–1314.
50 S. Ito and G. Prota, *Experientia*, 1977, **33**, 1118–1119.
51 S. C. Nicklisch, J. E. Spahn, H. Zhou, C. M. Gruian and J. H. Waite, *Biochemistry*, 2016, **55**, 2022–2030.
52 G. Maier, C. Bernt and A. Butler, *Biomater Sci*, 2018, 332–339.
53 R. T. Williamson, A. V. Buevich, G. E. Martin and T. Parella, *J. Org. Chem.*, 2014, **79**, 3887–3894.
54 J. March, *Advanced organic chemistry: reactions, mechanisms, and structure*, McGraw-Hill, New York, 1977.
55 Y. Ding and A. S. Hay, *Macromolecules*, 1996, **29**, 6386–6392.
56 J. Houk and G. M. Whitesides, *Tetrahedron*, 1989, **45**, 91–102.
57 R. Sato, S. Saito, H. Chiba, T. Goto and M. Saito, *Bull. Chem. Soc. Jpn.*, 2006, **61**, 1647–1651.
58 G. Odian, *Principles of polymerization*, John Wiley & Sons, 2004.
59 J. M. G. Cowie and V. Arrighi, *Polymers: chemistry and physics of modern materials*, CRC press, 2007.
60 M. D. Lechner, K. Gehrke and E. H. Nordmeier, *Makromolekulare chemie*, Springer, 2003.
61 F. Billmeyer, *Textbook of polymer science*, John Wiley & Sons, 1984.
62 C. Tschierske, in *Liquid Crystals: Materials Design and Self-assembly*, ed. C. Tschierske, Springer Berlin Heidelberg,

Berlin, Heidelberg, 2012, pp. 1–108. DOI: 10.1007/128_2011_267.
63 C. M. Schröter, L. D. Bangert and H. G. Börner, *ACS Macro Lett.*, 2024, **13**, 440–445.
64 M. A. North, C. A. Del Grosso and J. J. Wilker, *ACS Appl. Mater. Interfaces*, 2017, **9**, 7866–7872.
65 X. Zhang, H. Liu, L. Yue, Y. Bai and J. He, *J. Mater. Sci.*, 2020, **55**, 7981–7997.